

Design and test of post-seat weeding machine for paddy

Liang Tian, Chengmao Cao^{*}, Kuan Qin, Liangfei Fang, Jun Ge

(School of Engineering, Anhui Agricultural University, Hefei 230036, China)

Abstract: Aiming to solve problems in organic rice weeding a type of post-seat weeding machine was designed for rice paddies. The differences in the strengths and lengths of the root systems between the rice seedlings and the weeds were studied, and the motion track of the weeding wheel was analyzed to obtain the structural parameters of the weeding wheel. Then, the structural model of the weeding wheel was designed. The interaction process between the weeding wheel and soil in the paddy fields was simulated and analyzed based on the discrete element method, so as to investigate the working resistance change tendency of the weeding wheel and the orderliness of the soil disturbances. An orthogonal test was designed in this study, with three factors: the hoeing depth, the rotation rate of the weeding wheel, and the forward speed of the device. The influences of different operation parameters of the weeding machine on the weeding torque and soil disturbance speed were obtained based on a variance analysis of the test results. A multi-index comprehensive weighted scoring method was used to evaluate the simulation results. A soil bin test was conducted to verify the simulation results. Field experiments were carried out to test the working performance of the weeding machine. The comprehensive scoring results indicated that a better working performance of the weeding operation could be obtained when the hoeing depth was 50 mm, the rotation rate of the weeding wheel was 240 r/min, and the forward speed was 0.6 m/s. The results of the soil bin test were consistent with the simulation results. The results of the field experiment revealed that the weeding machine met the requirements for organic rice weeding. These results can provide a reference for the design of weeding machines for paddy fields.

Keywords: paddy field, weeding, structural parameters, discrete element method, soil

DOI: 10.25165/j.ijabe.20211403.5936

Citation: Tian L, Cao C M, Qin K, Fang L F, Ge J. Design and test of post-seat weeding machine for paddy. *Int J Agric & Biol Eng*, 2021; 14(3): 112–122.

1 Introduction

The application of herbicides is not allowed in organic rice production^[1], and weed control has become a major challenge. Mechanical weeding is an efficient and environmentally friendly method for weed management, and can meet the requirements for organic production systems^[2].

Japan is at the forefront of paddy field mechanical weeding technology^[3]. Weeding machines can be classified into riding weeders and walking weeders. The Mitsubishi Agricultural Machinery LVW-8 weeding machine^[4] and Heshi Industry RW50 weeding machine^[5] belong to riding weeders. The Hetong Industry MSJ-4 weeding machine^[6] and Meishan SMW weeding machine^[7,8] are riding weeders. Riding weeders are operated with high-speed rotating hoes or rake teeth for removing inter-row weeds, and intra-row weeds are removed by comb teeth or rotary weeding machines along the forward direction. Walking weeders remove inter-row weeds using a walking wheel or a follow-up weeding wheel, and the intra-row weeds are removed using a rotary weeding device^[9]. Research on weeding machines has been conducted in China following the achievements of other developed countries with regard to weeding machines. The

3SCJ-1 weeding machine for paddy fields was researched by Wang et al.^[10], and a light paddy field weeding machine with high-speed rotating rake blades was designed by Qi et al.^[11,12]. Several studies on weeding machines in paddy fields have been conducted in China. However, knowledge of the weeding machines remains lacking with regard to operations under different tillage conditions. In addition, the weeding machines are prone to excessive resistance and skidding during operation. Therefore, in order to improve the weeding efficiency and reduce the working resistance, it is necessary to analyze the interaction process between the blade and the soil in paddy fields, study the working resistance change tendency of the weeding blade during operation, and examine the orderliness of soil disturbances in paddy fields.

Soil tillage mechanisms are extremely complicated. The mechanical disturbance of soil is affected by many complex factors, such as the soil spatial variation, dynamics of the tillage machinery, and soil fragmentation. Therefore, it is difficult to analyze the soil disturbances by merely using traditional experimental methods. Moreover, the conditions of soil are complicated and variable. Furthermore, the experimental process is tedious, and it is difficult to achieve desired outcomes when studying the deformation, crushing, and stress states of the parts in contact with soil using the method of field experiment^[13]. Soil is typically composed of colloidal or condensed rock, as well as weathered mineral particles of different sizes (which determine the discreteness of the soil). Some errors have been observed in the movement, deformation, and tearing of soil during simulated tillage using the finite element methods (FEM) or smoothed particle hydrodynamics (SPH) methods. Cundall and Strack^[14] proposed a discrete element method (DEM) with discontinuity and an independent moving monomer as the research object. The motion and force of the

Received date: 2020-05-30 **Accepted date:** 2021-04-05

Biographies: Liang Tian, PhD, research interest: agricultural machinery, Email: 528394233@qq.com; Kuan Qin, PhD, research interest: agricultural machinery, Email: qinkuan@ahau.edu.cn; Liangfei Fang, PhD, research interest: agricultural machinery, Email: 30923663@qq.com; Jun Ge, PhD, research interest: agricultural machinery, Email: gejunahau@ahau.edu.cn.

***Corresponding author:** Chengmao Cao, PhD, Professor, research interest: agricultural machinery. School of Engineering, Anhui Agricultural University, Hefei 230036, China. Tel: +86-13696515592, Fax: +86-551-5786317, Email: ccm@ahau.edu.cn.

monomer were determined based on Newton's second law and the static force between the monomer and the monomer in contact with it. The discrete element method is used to study the soil disturbances and the forces of the soil-contacting parts of cultivated land, which treats the soil as a discontinuous unit, is similar to actual soil. Based on a virtual simulation analysis of push plates, Shmulevich et al.^[15] demonstrated that the discrete element method was more suitable for the analysis of high plastic deformations and particle flows in soil. Mustafa^[16] verified that the discrete element method could be used to study the disturbance behaviors of soil and the stresses of tools.

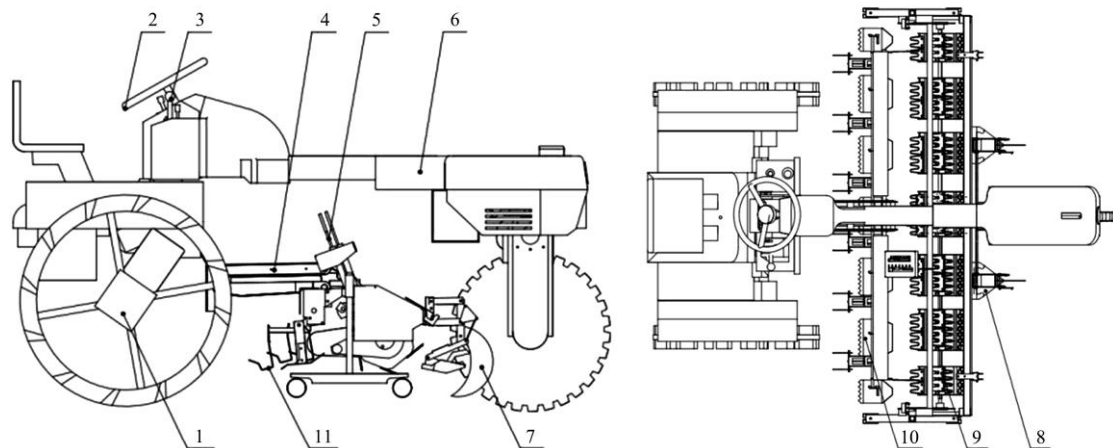
Most Asian countries grow wet rice, and the interaction effects of the water and soil are complex. Previous studies on the dynamic simulation of soil mechanical properties using the discrete element method have mainly focused on dry soil. These studies involve all aspects of soil model building and parameter selection, and determine the shear forces, local strain, and plasticity, based on

multiple indicators. However, studies on the interactions between paddy soil and machinery using the discrete element method have seldom been reported in works of literature. Therefore, this work aimed to study the interaction process between the weeding wheel and soil in paddy fields and design a type of weeding machine for paddy, so as to provide a theoretical basis for designing and controlling mechanical weeding device.

2 Materials and methods

2.1 Machine structure and working principle

The structure of the post-seat weeding machine for paddy devised in this study is illustrated in Figure 1. It is mainly composed of a walking wheel, steering wheel, speed adjustment device, suspension device, hoeing depth and speed adjustment device, device frame, anti-winding knife, depth-limiting plate, inter-row weeding device, scratch mud board, and intra-row weeding device.



1. Walking wheel 2. Steering wheel 3. Speed adjustment device 4. Suspension device 5. Hoeing depth and speed adjustment device 6. Device frame 7. Anti-winding knife 8. Depth-limiting plate 9. Inter-row weeding device 10. Scratch mud board 11. Intra-row weeding device

Figure 1 Structure of riding weeding-cultivating machine for paddy fields

To meet the requirements for weeding depth in different fields, the hoeing depth and speed adjustment device should be adjusted prior to field application. The machine is powered by a gasoline engine. During operation, the power was transmitted from the gasoline engine to the walking device and the weeding device, through which the machine moved ahead at a suitable speed. During the rotation of the weeding wheel, the rake teeth entered the soil to remove the inter-row weeds. After weeding, the rake teeth were raised off the ground, and the soil was thrown backward. The machine uses this method to loosen the soil and kill weeds.

2.2 Weeding mechanism

Rice, a major staple in China, is an annual gramineous plant. The crop is suited for growing in regions with a fairly high temperature, high humidity, and prolonged sunshine. Rice is characterized by a fibrous root system composed of a main root and secondary roots^[17]. The root growth of rice is gradual during the period of seedling establishment after transplanting. When a rice seedling is in the tillering stage, lateral expansion dominates the root system, and the root group within 20 cm is oblate. The number of rice roots varies with the variety of rice and the environment, up to 1000, and is generally approximately 200; the average length of roots is between 40-60 cm^[18]. After the heading stage, the roots completely stop growing, and the number of roots begins to decrease^[19,20].

There are many species of weeds in paddy fields in China; barnyard grass (*Echinochloa crusgalli*) and Chinese sprangletop

(*Letochoa chinensis*) are two typical malignant weeds. Barnyard grass belongs to Gramineae, which is similar to rice in appearance, and demonstrates a strong association with rice. Barnyard grass is the first malignant weed in paddy fields, and significantly affects the yield and quality of rice production^[21]. Chinese sprangletop is an annual gramineous weed. It is characterized by a high plant rate, dry growth and wet favor, a strong tillering ability, a tall height, a long symbiosis period with rice, and insensitivity to common herbicides. It is one of the malignant weeds in the main rice-producing areas worldwide, and its harm to farmlands is only inferior to that of barnyard grass^[22]. In this study, barnyard grass and Chinese sprangletop are considered as examples. The weeds mentioned below refer to barnyard grass and Chinese sprangletop.

Barnyard grass, Chinese sprangletop, and rice are all gramineous plants, and have ample similarities in their growth. The roots of barnyard grass and Chinese sprangletop are fibrous, including the main root and the secondary roots. Furthermore, they all undergo a growth cycle of a seedling stage, tillering stage, and heading stage. There is a time difference between weeds and rice in the growth and development periods. Although weeds grow in a similar manner to rice, they do not grow synchronously. Based on the asynchronous growth and development cycles of rice and weeds, this research analyzed the similarities and differences in root growth between seedlings and weeds, and expressed the weeding mechanism of the weeding machine.

The Gramineae weeds, such as barnyard grass and Chinese

sprangletop, began to germinate 3-5 d after rice transplanting, peaked on the 7th day, and rarely appeared after the 13th day^[23]. The rice seedlings entered the tillering stage at the end of the green period (approximately one week after transplanting). During this period, the rice seedlings developed a main root and secondary root, with a flat elliptical distribution of the root groups. In contrast, the weeds at this time were in the germination stage; a few weeds had just entered the seedling stage, with only one weak main root and unproduced secondary roots. During this period, the difference between the rice root system and weed root system was significant. The rice was more robust than the weeds, making weed removal relatively simple. When the weeds entered the tillering stage, the secondary roots began to proliferate, forming developed roots, and the difference between the roots of the weeds and those of rice gradually decreased. As weeds compete with rice for sunlight and nutrients, the more vigorous the weeds grow, the more nutrients they consume in the field, and consequently, the fewer nutrients available for the rice to absorb. The stronger the weeds grow, the more difficult the weeding. As a consequence, the cost of weed control increases. It can be seen from the above analysis that the best time for weeding in paddy fields is approximately one week after transplanting the rice crop, as the weeds are just beginning to grow and develop (different from the seedlings). As the weeds have not yet affected the growth of the seedlings, it is less difficult to remove them. The second weeding should be conducted approximately two weeks after transplanting, to remove the weeds that germinated after the first weeding. After two weeding operations, the newly emerging weeds in the paddy fields cause less interference, and cannot compete with the rice seedlings. One week after transplanting, the root depth of the rice seedlings was approximately 8-10 cm, and the root system diameters not exceeding 3 cm. In contrast, the root system of the weeds was only approximately 3-5 cm.

During the operation of the weeding machine in a paddy field, the actuator exerted a force when it touched the seedlings or weeds. This force continued to affect the plants in the paddy fields and was greater than the resistance of the soil to the root system of the plants. Thus, the plants were driven away from the original position in the soil by the weeding machine, and were pressed into the soil or removed. When the paddy field plants touch the weeding machine, the force on their roots is denoted as F . To facilitate the analysis, F is decomposed orthogonally; F_H is the horizontal force of F and F_V is the vertical force of F , as depicted in Figure 2.

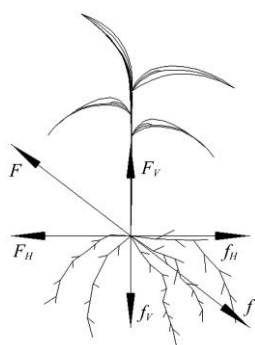


Figure 2 Orthogonal decomposition diagram of stress on plant root

During the growth of the rice plants, their roots crisscrossed the soil. When the plants tended to break away from the soil under the effects of external forces, the plants were prevented from moving by many forces, such as the friction force, shear force, and

water adsorption force of the paddy soil on their root systems. These forces were various and complex, and are denoted as the soil resistance f .

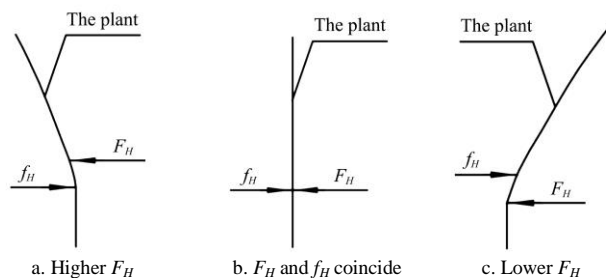


Figure 3 Effects of the horizontal force F_H on plant

In the horizontal direction, when F_H was extremely small, the plant was still under the effect of the horizontal soil resistance f_H . At this time, F_H and f_H were equal in intensity and opposite in direction, acting as mutual and reaction forces. When F_H was greater than the maximum soil resistance f_{Hmax} in the horizontal direction, the plant could not remain motionless. At this stage, the plant exhibited the following three modes of movement, as depicted in Figure 3 that 1) when the action point of F_H was higher than that of f_{Hmax} , the plant stalk was “pressed” to the soil, and the plant was buried in the soil or pulled off; 2) when the action point of F_H was coincident with the action point of f_{Hmax} , the plant was “pushed” by the soil, affecting the later stages of growth and development; 3) when the action point of F_H was lower than that of f_{Hmax} , the stalk of the plant was dragged into the soil along with the root systems, and the plant was buried in the soil.

In the vertical direction, when F_V was extremely small, the plant remained static under the effect of the vertical soil resistance f_V . At this time, F_V and f_V were equal in intensity and opposite in direction, and acted as mutual and reaction forces. When F_V was greater than the maximum soil resistance f_{Vmax} in the vertical direction, the plant could not remain motionless, and was “picked out” of the soil. The weeding machine should pick out weeds without affecting the seedlings, thereby meeting the mathematical expression as follows:

$$f_{v_w} \leq F_V \leq f_{v_r} \tag{1}$$

where, f_{v_w} denotes the maximum soil resistance in the vertical direction of the weeds; f_{v_r} denotes the maximum soil resistance in the vertical direction of the rice seedlings.

2.3 Principle of weeding wheel

The weeding wheel is powered by a gasoline engine, and the structure of the weeding rake teeth is considered to improve the weeding performance and adequately prepare the land for paddy fields. When the weeding wheel rotates in a paddy field, the paddy soil is disturbed. More specifically, the lower layer of the soil in the paddy field becomes the upper layer with the rotation of the weeding rake teeth, and is mixed with water. Consequently, the lower soil is fully mixed with the upper soil of the paddy field under the action of the water flow and scour, so as to achieve the purpose of cultivation. While the weeding wheel is working in the field, the weeding rake teeth pulls the root systems of the weeds out of the soil and presses the stems and leaves of the weeds under the paddy field soil. The growth of the weeds was destroyed. Then the absorbing nutrients and performing photosynthesis of weeds were prevented. Thus, weed control can be achieved.

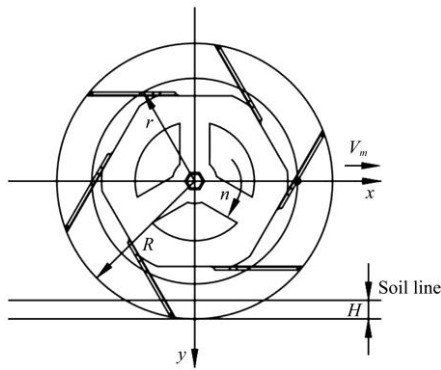
The weeding teeth do not have a side cutting edge and tangent cutting edge like that of a rotary blade. Instead, it comprises a steel plate, similar to a plane sheet, with multiple notches at the

front end. When the weeding teeth contact the soil, it demonstrates a face contact rather than a line contact. With the rotation of the knife roll, the blade moves downward and backward to the field surface. Instead of sliding into the soil, the blade exerts forces on the ground surface to squeeze and push the soil sideways with fluidity, so as to uproot or bury the weeds. As the blade weeds by pushing and pressing, although the sliding angle is extremely small, it does not cause the phenomenon that the blade shaft is wrapped in grass. In particular, such a form of action between the blade and field surface can only be applied to a field surface with mobility and that is composed of water, mud, and weeds^[24].

2.4 Motion analysis of weeding wheel

The weeding wheel is powered to move around an axis and moves in the forward direction with the weeding device. The motion of the weeding wheel can be regarded as the combined motion of a uniform linear motion and uniform circular motion around the axis.

A Cartesian coordinate system is illustrated in Figure 4, where the rotation center of the weeding wheel is considered as the coordinate origin. The positive direction of the X-axis is the forward direction of the machine, and the positive direction of the Y-axis is vertical and downward. Point D is a point on the top of the weeding wheel, and the initial position of point D is on the X-axis.



Note: v_m is the forward speed of the weeding machine, m/s; n is the rotation rate of the weeding wheel, r/min; R is the rotation radius of the weeding wheel, mm; r is the radius of the weeding wheel, mm; H is the hoeing depth, mm.

Figure 4 Schematic analysis of weeding wheel motion

The motion of point D is a combined linear and circular motion; thus, the equation for the motion trajectory of point D can be represented as follows:

$$\begin{cases} X = v_m t + r \cos \omega t \\ Y = r \sin \omega t \end{cases} \quad (2)$$

$$\omega = \frac{2\pi n}{60} \quad (3)$$

where, r is the radius of weeding wheel, mm; R is the rotation radius of weeding wheel, designed as 185 mm; v_m is the forward speed of weeding machine, m/s; n is the rotation rate of weeding wheel, r/min; t is the rotating time of the rotating parts (with the Y-axis as the starting point); H is the hoeing depth, mm.

The split velocity of point D in the horizontal and vertical directions is as follows:

$$\begin{cases} v_x = dx / dt = v_m - \omega r \sin \omega t \\ v_y = dy / dt = \omega r \cos \omega t \end{cases} \quad (4)$$

The instantaneous velocity of point D is as follows:

$$v_D = \sqrt{v_x^2 + v_y^2} \quad (5)$$

Substituting Equation (4) into Equation (5), an equation can be

obtained as follows:

$$v_D = \sqrt{v_m^2 + \omega^2 r^2 - 2v_m \omega r \sin \omega t} \quad (6)$$

Here, λ is used to define the ratio of the peripheral speed of the weeding wheel to the forward speed of the device. The weeding speed ratio λ is defined as follows:

$$\lambda = v_0 / v_m \quad (7)$$

$$v_0 = \omega r \quad (8)$$

where, v_0 is the peripheral speed of the weeding wheel, m/s.

From Equations (7) and (8), Equation (9) was obtained:

$$\omega r = \lambda v_m \quad (9)$$

Substituting Equation (9) into Equations (4) and (6), then

$$v_x = v_m - \lambda v_m \sin \omega t \quad (10)$$

$$v_D = \sqrt{v_m^2 + \lambda^2 v_m^2 - 2\lambda v_m^2 \sin \omega t} \quad (11)$$

Evidently, the value of λ directly affects the motion trajectory of the weeding wheel in the soil and the working state of the weeding wheel rake teeth.

If $\lambda < 1$, $v_0 < v_m$, regardless of the blade movement, $v_x > 0$ always holds, and the horizontal velocity direction of the blade at each point is always the same as the forward direction of the device. The motion trajectory of the blade is a short cycloid. Thus, instead of compressing the soil backward, the weeding wheel only pushes the soil forward with the blades. This is contrary to the working principle of the weeding wheel, and therefore, the weeding wheel does not function properly.

If $\lambda = 1$, $v_0 = v_m$, regardless of the blade movement, $v_x \geq 0$ always holds, and its motion trajectory is a standard cycloid. The motion of the weeding wheel is similar to that when $\lambda < 1$, the wheel does not function in a similar way.

If $\lambda > 1$, $v_0 > v_m$, when the blade is turned to a suitable position, $v_x < 0$ holds. It appears that the direction of the horizontal component of the absolute movement speed of the blade at point D is opposite to the forward direction of the device. The motion trajectory of the weeding wheel is a trochoid, and the weeding wheel can extrude the soil backward. In the weeding process, the motion track of each point on the weeding wheel should be a cycloid; in other words, the peripheral speed v_0 should be greater than the forward velocity v_m of the weeding device.

To ensure that the weeding machine does not omit weeds during operation, the forward distance of the device should be less than or equal to the circumference of weeding wheel when the weeding wheel rotates a circle, which can be represented as follows:

$$v_m t \leq 2\pi r \quad (12)$$

$$t = 2\pi / \omega \quad (13)$$

where, t is the time required for the weeding wheel to rotate a cycle, s.

Substituting Equations (3) and (13) into Equation (12), which can be represented as follow:

$$v_m \leq \pi r n / 30 \quad (14)$$

2.5 Structural design of weeding wheel

2.5.1 Width of weeding wheel

The row spacing of the rice seedlings was 300 mm^[25]. To reduce the damage to the rice seedlings during weeding operation, sufficient space was provided between the weeding wheel and rice seedlings. Therefore, the width of the weeding wheel was designed as 220 mm.

2.5.2 Radius of weeding wheel

The power of the weeding wheel is transmitted by the

transmission shaft. Ideally, the designed radius of the weeding wheel not only ensures the effective removal of weeds, but also prevents the bottom of the gearbox from coming in contact with the soil and increasing the resistance. To avoid the entangling of weeds during operation, the circumference of the weeding wheel should be greater than the height of weeds. This can be represented mathematically, as follows:

$$2\pi r \geq L \quad (15)$$

where, L is the weed height, mm.

According to a previous study^[26], the height of weeds before ridge sealing is generally not more than 250 mm, by substituting into Equation (15), $r \geq 39.8$ mm is obtained. Thus, the radius of the weeding wheel is 125 mm, which can ensure that the weeds are not wrapped.

2.5.3 Number and length of weeding rake teeth

To reduce abrasion and power consumption, ensure the weeding effect, the weeding wheel should be in an absolute rolling state. However, the weeding wheel tends to inevitably slip, owing to the complex and changeable working environment in paddy field^[27]. The slip degree of the weeding wheel can be expressed by the slip rate k , as follows:

$$k = (v_0 - v) / v_0 \quad (16)$$

$$\begin{cases} v_0 = 2\pi n r_0 / 60 \\ v = 2\pi n / 60 \\ r = s / 2\pi \end{cases} \quad (17)$$

where, v_0 is the theoretical peripheral speed of the weeding wheel, m/s; r_0 is the theoretical rolling radius of the weeding wheel, m; v is the actual peripheral speed of the weeding wheel, m/s; n is the rotation speed of the weeding wheel, r/min; r is the rolling radius of the weeding wheel, m; S is the forward distance of the device movement while the weeding wheel rotates a circle, m.

In the process of turning the weeding wheel forward, if the number of rake teeth in the weeding wheel is lower than necessary, some weeds will not be removed; in contrast, if the number of rake teeth exceeds that necessary, the weeding wheel will be overweight. If the rotation radius of the rake teeth of the weeding wheel is too much large, some weeds will be omitted. Therefore, the weeding wheel requires the determination of a reasonable rotation radius for the rake teeth, as well as the number.

To ensure that all inter-row weeds in paddy fields can be removed during operation, the sum of the working length of all rake teeth of the weeding wheel should not be less than the forward distance of the device movement while the weeding wheel rotates in a circle. This can be expressed as follows:

$$bN \geq s \quad (18)$$

Substituting Equation (18) into Equation (17), which can be represented as follow:

$$bN \geq 2\pi r_0(1 - k) \quad (19)$$

In Equation (19), b is the length of the rake tooth, mm; N is the number of rake teeth.

To avoid soil-blocked for the weeding wheel during operation, the number of rake teeth should not be excessive. It can be seen from Equation (19) that in weeding machine with shorter rake teeth, the slip rate tends to increase; when the number of rake teeth decreases, the stability of the weeding machine appears to be poor. After comprehensive consideration, the number of rake teeth N was set as 6, and the length of a rake tooth b was determined as follows:

$$b \geq \frac{1}{3} \pi r_0(1 - k) \quad (20)$$

The slip rate of agricultural machinery in field operation is 3%-8%, and appears to be more than 15% in paddy field operation; therefore, power is likely to be wasted^[28]. In the design, the slip rate k was considered as 25% and the number of rake teeth N was 6; thus, the length of the rake teeth b in the weeding wheel was determined as 120 mm.

3 Analysis of discrete element method of weeding wheel

3.1 Weeding wheel model

It is tedious and complicated to process graphics using the discrete element method software (EDEM). For this reason, EDEM is unsuitable for complex 3D modeling. To ensure the accuracy of the simulation analysis, the weeding wheel was modeled at a 1:1 ratio using the 3D modeling software Unigraphics NX. Then, the 3D model was imported into the EDEM software in the .igs format.

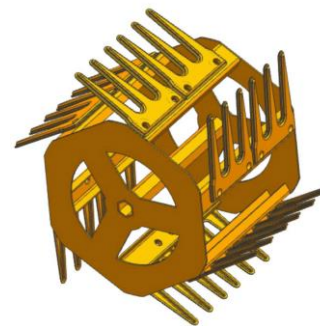


Figure 5 3D model of weeding wheel

3.2 Soil-water model

In a discrete element simulation, a subtle decrease in the particle size generally causes an enormous increase in the simulation time. To reduce the simulation time, the particle size used in a discrete element simulation is generally larger than the actual size^[29,30]. In this study, the soil particles were appropriately enlarged to save simulation time. Soil particles with a radius of 5 mm were used to simulate the paddy soil.

3.2.1 Soil contact model

The contact model is an important foundation of the discrete element method, and its essence concerns the results of an elastic-plastic analysis of the contact mechanics of a solid under a quasi-static state. The analysis and calculation of the contact model directly determine the forces and motions of the particles. Different contact models must be established for different simulation objects to improve the accuracy of the simulation results^[31].

The Hertz-Mindlin model with Johnson-Kendall-Roberts (JKR) cohesion is a cohesive contact model. Using this model, the mechanical behavior of wet particles can be well-simulated by considering the influence of the van der Waals force in the contact area^[32]. Therefore, this study adopts this model to study a soil particle model for paddy fields. In this model, the understanding of the normal elastic contact force is based on the JKR theory as published in 1971.

To study the tangential force, normal dissipation force, and tangential dissipation force, the Hertz-Mindlin with JKR cohesion contact model uses the same calculation method as the Hertz-Mindlin non-slip contact model.

The calculation of the friction force in this model is different from that in the Hertz-Mindlin no-slip contact model, and depends on the part of the force that is repulsed by the JKR normal force.

Therefore, as the force exerted on the contact surface of the bonded part increases, the friction provided by the JKR model in EDEM also increases.

The amount of force required to separate two paddy soil particles depends on the liquid surface tension γ_s and wetting angle θ , as follows:

$$F_{pullout} = 2\pi r_s \cos(\theta) \sqrt{R_i R_j} \quad (21)$$

The equation for calculating the JKR maximum force is as follows:

$$F_{pullout} = -\frac{3}{2} \pi r R \quad (22)$$

Under the condition that the EDEM particle size does not change, this equation can be used to estimate the JKR surface energy parameters^[33].

3.2.2 Soil-water simulation model

The surface soil of a paddy field was saturated when the weeding wheel was in operation. In this study, the contact model was initially determined in the discrete element simulation system, and two different sizes of particles were established to represent water and soil, respectively. Then, the water particles were infiltrated into the soil particles to simulate the formation process of natural mud and water. Finally, a soil model similar to the soil of paddy fields was formed, that is, upper layer with a single water particle, middle layer representing a saturated soil layer (as a mixture of water particles and soil particles), and lower layer of soil with a small amount of water.

In the EDEM software, the model parameters are mainly categorized into material and contact parameters. The material parameters include the shear modulus, density, and Poisson ratio. The contact parameters mainly include the friction coefficient and the recovery coefficient between materials. The material parameters and contact parameters can be obtained through field measurements, experimental measurements, and literature references. The density of water is 1000 kg/m^3 , Poisson ratio is 0.5, and shear modulus is 0. In view of the requirement that the shear modulus cannot be 0 in EDEM, the shear modulus is determined as 100 MPa, based on the literature on discrete element^[34]. The Poisson ratio, shear modulus, and density of the soil model were set at 0.5, 100 MPa, and 2000 kg/m^3 , respectively, and the surface energy was set at 0.15 J/m^3 . The Poisson ratio of the water model was set at 0.5. The shear modulus was set at 100 MPa, and the density at 1000 kg/m^3 .

3.3 Working model of weeding wheel in EDEM

In this study, the simulation of the weeding operation of the weeding wheel was established by using the EDEM software. To meet the requirements of the weeding operation, a virtual soil bin with a length \times width \times height of $1000 \text{ mm} \times 450 \text{ mm} \times 100 \text{ mm}$ was designed in EDEM, and a 20 mm thick water layer was created on the soil bin. The weeding wheel model was located at one end of the soil bin after being imported from EDEM. The hoeing depth, rotation speed of the weeding wheel, and forward speed of the device were set in EDEM. The material of the weeding wheel was steel. The Poisson ratio, shear modulus, and density were 0.3, $7.0 \times 10^4 \text{ MPa}$, and 7800 kg/m^3 , respectively. In the simulation model, 50 060 soil particles and 149 850 water particles were created. Soil particles were generated at the beginning of the simulation. After the soil particles settled and stabilized, water particles were generated above the soil particles. Following the penetration process, where in the water particles flow downward into and through the soil particles, the weeding wheel began to

move. To ensure continuity of the simulation, the fixed time step was $2.07 \times 10^{-5} \text{ s}$, it was 30% of the Rayleigh time step. After the simulation was complete, the simulation result data were exported and analyzed in the EDEM post-processing tool module.

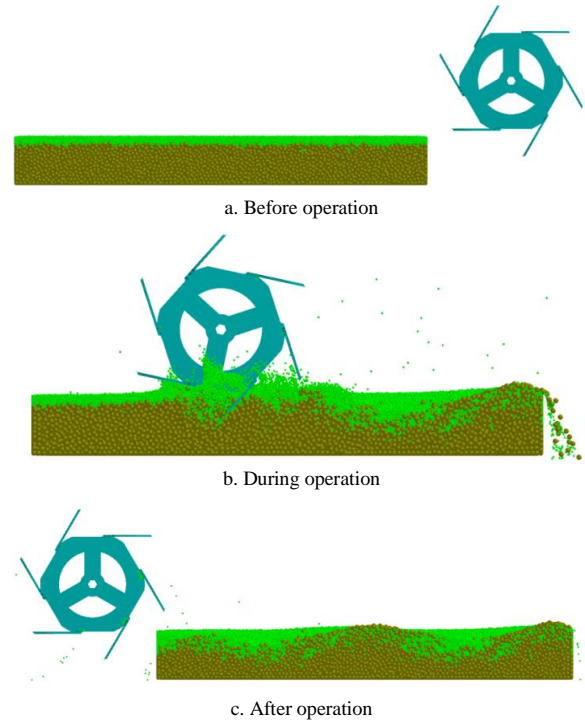


Figure 6 EDEM simulation model of weeding wheel

4 Results and discussion

4.1 Design of simulation experiment

To explore the weeding effect of the weeding wheel with different working parameters and the energy consumption of the device during operation, the working process of the weeding wheel was simulated and analyzed using the discrete element method software EDEM. As it was not possible for the weeding effect and energy consumption of the device to be represented directly in EDEM, in this study, the soil disturbance speed and weeding torque were used as indices to indirectly evaluate the weeding effect and energy consumption. The torque of the weeding wheel during the weeding operation reflects its penetrability and the energy consumption of the entire device, and the soil disturbance reflects the weeding effect.

In this study, the hoeing depth, rotation speed of the weeding wheel, and forward speed of the weeding machine were selected as the experimental factors. The weeding torque and soil disturbance speed were used as the indices for assessing the experiment. In addition, an orthogonal experimental method was applied to design the experiment. Ultimately, the interaction process between the weeding wheel and soil was simulated and analyzed, and the evaluation indices were evaluated comprehensively using a multi-objective optimization design method.

The maximum torque of the weeding wheel during the interaction between the weeding wheel and soil-water model was defined as the maximum weeding torque (hereinafter, referred to as the weeding torque). It has been demonstrated that as the weeding torque decreases, the resistance of the weeding wheel tends to decreasing, and the energy consumption of the operations also decreases. The maximum speed of the soil particles was defined as the maximum soil disturbance speed (hereinafter, referred to as the soil disturbance speed), and varied with the rotation of the

weeding wheel. In general, when the soil disturbance speed increased, the weeding performance was improved with a greater extent of soil disturbance.

According to the differences in length between the rice seedlings and weeds during growth, three levels of the hoeing depth were selected: 30 mm, 40 mm, and 50 mm. According to the gear transmission ratio and actual production operation requirements, three rotation speeds of the weeding wheel were selected: 120 r/min, 180 r/min, and 240 r/min. According to the actual production operation requirements, three forward speeds of the weeding machine were selected: 0.3 m/s, 0.6 m/s, and 0.9 m/s. A three-factor three-level orthogonal experiment table $L_9(3^3)$ was used to arrange the sequence of the simulation experiment. The orthogonal simulation experiment was conducted in accordance with the above experimental scheme. The experimental factors and levels are presented in Table 1, the test arrangements and results are presented in Table 2, and a variance analysis of the test results is presented in Table 3.

Table 1 Experimental factors and levels

Levels	Factors		
	Hoeing depth A/mm	Rotation speed B/r min ⁻¹	Forward speed C/m s ⁻¹
1	30	120	0.3
2	40	180	0.6
3	50	240	0.9

Table 2 Test arrangements and results

Test No.	Factors			Weeding torque $\eta_1/N\ m$	Soil disturbance speed $\eta_2/m\ s^{-1}$	Comprehensive score Z
	A	B	C			
1	1	1	1	0.9172	2.6771	0.2500
2	1	2	2	1.7828	4.4458	0.3367
3	1	3	3	2.0954	4.6293	0.3207
4	2	1	2	0.9332	3.0290	0.2848
5	2	2	3	1.6138	5.5147	0.4669
6	2	3	1	3.0334	9.4334	0.7149
7	3	1	3	1.2304	3.3446	0.2842
8	3	2	1	2.7097	6.6883	0.4658
9	3	3	2	3.1440	9.8909	0.7500

Table 3 Variance analysis of test results

Sources	A	B	C	
η_1	K_1	4.7954	3.0808	6.6603
	K_2	5.5804	6.1063	5.8600
	K_3	7.0841	8.2728	4.9396
	k_1	1.5985	1.0269	2.2201
	k_2	1.8601	2.0354	1.9533
	k_3	2.3614	2.7576	1.6465
	R	0.7629	1.7307	0.5736
Influence degree	B>A>C			
Optimal combination	$A_1B_1C_3$			
η_2	K_1	11.7522	9.0507	18.7985
	K_2	17.9771	16.6488	17.3657
	K_3	19.9238	23.9536	13.4886
	k_1	3.9174	3.0169	6.2662
	k_2	5.9924	5.5496	5.7886
	k_3	6.6413	7.9845	4.4962
	R	2.7239	4.9676	1.7700
Influence degree	B>A>C			
Optimal combination	$A_3B_3C_1$			

4.2 Simulation experiment results

By using the EDEM post-process module to interpret the simulation results, the position and velocity distribution of the soil could be determined. Figure 7 depicts that after the rake teeth of the weeding wheel were put into the soil, the rake teeth compressed the soil, and the soil on the outer side of the rake teeth collapsed under the action of the extrusion pressure^[35]. As the rake teeth moved the soil backward, the inner side of the rake teeth did not participate in soil extrusion even though it touched the soil; thus, the soil deformation on the inner side of the rake teeth was not evident.

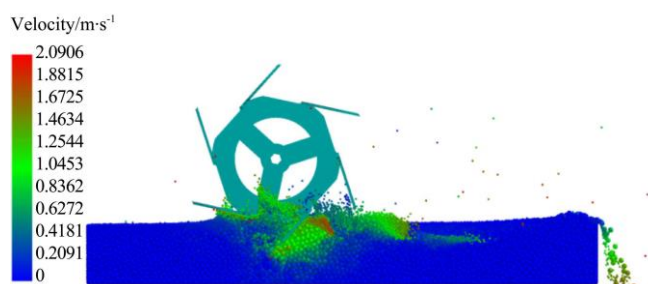


Figure 7 Distribution of soil-water speed during weeding

When the weeding wheel rotated in the paddy field, it played the role of not only weeding, but also hoeing. During the process of tillage, the weeding rake teeth were completely in contact with the soil of the paddy field, such that the soil and water layers were disturbed after being stirred and mixed. Soil tillage and soil disturbances in paddy fields can improve soil productivity by loosening the soil; they preserve nutrients for crops to enhance nutrient uptake, and improve crop root growth.

The process of soil disturbance can be observed from the experiments. First, the weeding rake teeth pushed and rolled the soil forward and downward, and then threw the soil backward and upward. Eventually, a soil ridge was formed during the process of weeding. In the first stage of weeding, the weeding rake teeth contacted the paddy soil and squeezed it laterally until the soil failed, deformed, and broke. This was known as the soil crushing stage. During this stage, the weeds in the paddy field were pressed into the soil and pushed away from their original positions by the weeding rake teeth. Thus, the grasping strength of the root systems of the weeds significantly decreased owing to the soil fragmentation and friability. Consequently, the efficiency of weeding was improved in the following stages. Subsequently, the soil was displaced to the lowest point of the rake teeth. This process was defined as the excavation stage. At this stage, the weeds were cut by the rake teeth together with the soil, and the soil was further loosened. The root systems of the weeds were damaged, and the stems and leaves were cut off. Finally, in the soil throwing stage, the chopped weeds were scattered to the rear along with the soil by the weeding rake teeth. During the process, the weeding rake teeth gradually rotated from the lowest point to the highest point, bringing the lower layer of the soil to the surface so that it could be completely mixed with the water layer. As a result, a soil ridge was formed at the back end of the weeding rake teeth, and the root systems of the weeds were completely pulled out of the soil. Accordingly, weed control was accomplished.

4.3 Analysis of simulation results

4.3.1 Extreme difference analysis of simulation results

The analysis of the weeding torque in the extreme difference analysis (Tables 2 and 3) show that:

- (1) The range (R) of the weeding torque in the rotation speed

of the weeding wheel was the largest. Therefore, the different rotation speeds of the weeding wheel had a greater effect on the weeding torque; the weeding torque was the smallest when the rotation speed was 120 r/min, was moderate when the rotation speed was 180 r/min and was at its maximum when the rotation speed was 240 r/min.

(2) With an increase in the hoeing depth, the weeding torque increased slightly.

(3) With an increase in the forward speed of the weeding machine, the weeding torque decreased gradually and insignificantly.

The analysis of the soil disturbance speeds in the extreme difference analysis (Tables 2 and 3) show that:

(1) The disturbances caused by the operation of the weeding wheel at different rotation speeds were different. The minimum disturbance was caused by the operation of the weeding wheel at 120 r/min, a moderate-level disturbance was caused by the operation of the weeding wheel at 180 r/min, and maximum disturbance was caused by the operation of the weeding wheel at 240 r/min.

(2) With an increase in the hoeing depth, the change in the soil disturbance due to the weeding wheel gradually increased.

(3) The soil disturbance caused by the weeding wheel decreased with an increase in the forward speed of the device.

From the analysis of the extreme differences in the factors in Table 3, the degree of influence of the factors on the weeding torque could be ranked in the following order: rotation speed of the weeding wheel>hoeing depth>forward speed of the device. The degree of influence of the factors on the soil disturbance speed could be ranked as follows: rotation speed of the weeding wheel>hoeing depth>forward speed of the device.

4.3.2 Multi-index comprehensive weighted score

As the optimal parameter combinations of the various factors of the weeding wheel under different indices could not be directly determined, it was necessary to comprehensively consider the degree of influence of each factor on the different indices to determine the optimal parameter combination.

To select the best combination of factors while considering the two indicators (weeding torque and soil disturbance speed), a comprehensive scoring standard^[36] was established. In this study, a mapping function and multi-index comprehensive weighted evaluation method were established to evaluate the two indices.

For the weeding torque, the mapping was determined as follows:

$$f_1(x_i) = \frac{x_{\max} - x_i}{x_{\max} - x_{\min}} (x_{\min} \leq x_i \leq x_{\max}) \quad (23)$$

where, $f_1(x_i)$ denotes the mapping and scoring function of the weeding torque, with the value range [0,1]; x_i is the weeding torque value of test i , N m; x_{\max} is the maximum value of the weeding torque in the test results, N m; and x_{\min} is the minimum value of the weeding torque in the test results, N m. As the weeding torque decreases, the comprehensive score increases.

For the soil disturbance speed, the mapping was determined as follows:

$$f_2(y_i) = \frac{y_{\max} - y_i}{y_{\max} - y_{\min}} (y_{\min} \leq y_i \leq y_{\max}) \quad (24)$$

where, $f_2(y_i)$ is the mapping and scoring function of the soil disturbance speed, with the value range [0,1]; y_i is the soil disturbance speed of test i , m/s; y_{\max} is the maximum value of the soil disturbance speed, m/s; y_{\min} is the minimum value of the soil

disturbance speed in the test results, m/s. As the soil disturbance speed increases, the comprehensive score increases.

The main purpose of the weeding machine's work was to remove field weeds, and the weight of the soil disturbance speed was greater than the weeding torque. After comprehensive analysis, the optimal weight allocation of the weeding torque and soil disturbance speed^[34] was determined as $\omega_1=0.25$, $\omega_2=0.25$.

The comprehensive weighted score Z_i for each set of tests can be expressed as follows:

$$Z_i = \omega_1 f_1(x_i) + \omega_2 f_2(y_i) \quad (25)$$

According to the data in Table 2 and Equation (25), a better performance of the weeding wheel can be obtained when the hoeing is 50 mm, rotation speed of the weeding wheel is 240 r/min, and forward speed of the implement is 0.6 m/s.

4.4 Discussion

The effects of the rotation speed of the weeding wheel on the weeding torque and soil disturbance speed were evident. A higher rotation speed of the weeding wheel resulted in a higher weeding torque, and a greater energy consumption of the weeding wheel during operation. However, as the soil disturbance speed increased, the weeding performance improved. When other conditions remained unchanged, the frequency of interaction between the weeding wheel and soil was enhanced by increasing the rotation speed of the weeding wheel, as the weeding wheel acted on more soil; the soil disturbance and torque of the weeding wheel increased accordingly.

Meanwhile, the effect of the hoeing depth on the weeding torque and soil disturbance speed was not evident. As the hoeing depth increased, the weeding torque increased, and the energy consumption of the weeding wheel during operation also increased; as the hoeing depth increased, the soil disturbance speed increased, and the weeding effect was enhanced. When the other conditions were not varied, an increase in the hoeing depth caused the weeding wheel to act on more soil, and the soil disturbance and torque of the weeding wheel were increased. However, during the operation of the weeding machine, the soil stirred by the weeding wheel was composed of soft and non-viscous mud with high moisture content. Therefore, when the hoeing depth increased, the weeding wheel tended to act on more soil, and the weeding torque did not increase significantly.

The forward speed of the device had no evident effect on the weeding torque and soil disturbance speed. As the forward speed of the machine decreased, the weeding torque increased, and the energy consumption of the weeding wheel during operation increased; as the forward speed of the machine decreased, the soil disturbance speed increased, and the weeding effect was enhanced. When the other conditions were not varied, the lower the forward speed of the machine, the longer the time the weeding machine worked on the same distance, and the greater the amount of soil it affected; therefore, the energy consumption and soil disturbance speed increased.

5 Test validation

To verify the accuracy of the simulation tests, a soil bin test device was designed for the paddy field weeding machine. The structure of the soil bin test device is illustrated in Figure 8. It was mainly composed of a weeding wheel, fixed soil bin, removable frame, and pair of rails. The length \times width \times height of the soil bin was 6000 mm \times 800 mm \times 500 mm. The weeding wheel was mounted on the removable frame, which moved along the rails in the soil bin. During operation, the speed control motor drove

the removable frame movement to complete the advancing process of the weeding machine. The execution motor transmitted power to the rotating shaft through the chain, and drove the weeding wheel to rotate.



Figure 8 Soil bin test device

5.1 Test conditions and indicators

On May 29, 2020, the soil bin tests were conducted at the Mechanical and Electrical Engineering Park of Anhui Agricultural University. Before the experiments, preparation work was completed for the paddy soil environment in the soil bin. Owing to the limitation of the test conditions, the weeds were cultivated in the simulated paddy field environment in the soil bin by artificial spreading. The selected weed variety was barnyard grass, as it is one of the most common and harmful weeds in paddy fields.

To intuitively reflect the working effect and energy consumption of the weeding wheel, the weeding rate and weeding torque were used as indicators to determine the performance of the weeding wheel.

The weeding rate can be defined as follows:

$$\eta = \frac{Z - Z_1}{Z} \times 100\% \tag{26}$$

where, η is the weeding rate; Z is the total number of weeds between the rice rows in the test area; Z_1 is the total number of weeds remaining between the rice rows in the test area after weeding.

The weeding torque in soil bin test refers to the torque received by rotating shaft of the weeding wheel during test. As the weeding torque increases, the resistance of the weeding wheel increases, and the energy consumption during weeding also increases.

5.2 Test method

First, the speed of the weeding wheel was calibrated according to the test requirements. Then, the removable frame was moved along the rails in the soil bin at a speed of 0.3-0.9 m/s by a frequency modulation console. The weeding test was conducted for the different hoeing depth, rotation speeds of the weeding wheel, and forward speeds of the removable frame.

The weeding rate represents the percentage of weeds removed (the broken, buried, or floating weed roots in the test area were considered as removed weeds, whereas the weed roots that were connected to the mud surface, and the weeds that could continue to grow were not considered as removed weeds). The number of weeds in the test area was counted before weeding. After the weeding test was completed, the numbers of removed and non-removed weeds were counted. Each group of data was collected three times, and the average was calculated.

The numbers of weeds between rows were measured before and after the test in the test area, and were input into Equation (26) to determine the weeding rate between rows. A torque sensor was

installed on the removable frame, and collected the torque received by the rotating shaft when the weeding wheel was in operation.

5.3 Test Scheme

To verify the accuracy of the simulation tests, the factors and levels presented in Table 1 were used for the soil bin tests, which were consistent with the simulation tests. The three-factor three-level orthogonal test table $L_9(3^3)$ was used to arrange the sequence of the soil bin tests, which were conducted in accordance with the above test project. The test arrangements and results are presented in Tables 4 and 5.

5.4 Analysis of test results

The results of the orthogonal test are listed in Table 3. The range analysis of the test results (Tables 4 and 5) show that, with respect to the degree of influence of the weeding torque, the rotation speed of the weeding wheel exhibited the most significant influence, followed by the hoeing depth. In contrast, the forward speed exhibited the least significant influence. The optimal combination was $A_1B_1C_3$, when the rotation speed of the weeding wheel was 120 r/min, hoeing depth was 30 mm, and forward speed was 0.9 m/s; moreover, the power consumption of the weeding wheel was the least.

Table 4 Soil bin test results

Test No.	Factors			Weeding torque ζ_1 /N m	Weeding rate ζ_2 /%
	A	B	C		
1	1	1	1	3.8033	95.25
2	1	2	2	5.4372	98.30
3	1	3	3	6.4691	98.63
4	2	1	2	3.9277	96.10
5	2	2	3	4.9514	98.92
6	2	3	1	8.1685	99.44
7	3	1	3	4.5345	97.65
8	3	2	1	7.1943	99.25
9	3	3	2	8.7379	99.72

Table 5 Variance analysis of the soil bin test results

Sources		A	B	C
ζ_1	K_1	15.7096	12.2655	19.1661
	K_2	17.0476	17.5829	18.1028
	K_3	20.4667	23.3755	15.9550
	k_1	5.2365	4.0885	6.3887
	k_2	5.6825	5.8610	6.0343
	k_3	6.8222	7.7918	5.3183
	R	1.5857	3.7033	1.0704
Influence degree		B>A>C		
Optimal combination		$A_1B_1C_3$		
ζ_2	K_1	292.18	289.00	294.19
	K_2	294.46	296.47	294.12
	K_3	296.62	297.79	295.20
	k_1	97.39	96.33	98.40
	k_2	98.15	98.82	98.06
	k_3	98.87	99.26	98.04
	R	1.48	2.93	0.36
Influence degree		B>A>C		
Optimal combination		$A_3B_3C_1$		

In terms of the degree of influence of the weeding rate, the rotation speed of the weeding wheel exhibited the most significant influence, followed by the hoeing depth, and then the forward speed. The optimal combination was $A_3B_3C_1$, when the rotation

speed of the weeding wheel was 240 r/min, hoeing depth was 50 mm, and forward speed was 0.3 m/s; under these circumstances, the weeding rate was the highest.

The weeding torques obtained from the simulation tests were not completely consistent with the weeding torques measured in the soil bin tests. Owing to the friction between the mechanisms, the torque measured by the torque sensor was greater than the torque received by the rotating shaft of the weeding wheel. The working environment simulated by the simulation tests was ideal, and the interactions between the weeding wheel rake teeth and weeds were not considered. Therefore, the weeding torques obtained by the simulation tests were slightly smaller than those obtained from the weeding wheel rotation shaft. Therefore, there were some deviations between the weeding torques obtained by the simulation tests and those measured by the soil bin tests. However, regardless of simulation tests or soil bin tests, the weeding torque was an important factor in determining the energy consumption of the weeding machine during operation. Changes in the weeding torque can reflect the energy consumption of the weeding wheel during operation.

The conclusions obtained from the simulation tests were consistent with those obtained from the soil bin tests, proving the feasibility of the modeling and simulation methods adopted in this study.

5.5 Field experiment

To verify the weeding performances of the weeding machine designed in this study, field experiments were conducted in Fenghuang Town, Fengtai County, Huainan City, Anhui Province.

In the field experiments, the weeding rate, rice seedling damage rate, and working fuel consumption were selected as the evaluation indices. The working parameters were selected based on the above mentioned conclusions. The hoeing depth was 50mm, rotation rate of the weeding wheel was 240 r/min, and forward speed was 0.6 m/s.

The weeding rate was obtained using Equation (26). The rice seedling damage rate was the percentage of the damaged rice seedlings in the test fields. Before the field tests, the number of rice seedlings in each area was counted. After the weeding tests, the test areas were surrounded by thin rope, and the numbers of damaged and undamaged rice seedlings were counted. The data of each group were collected three times, and the average was calculated. The values of the oil dial were recorded before and after the weeding tests, and the working fuel consumption of the weeding machine was represented by the difference in the values of the oil dial. The overall index was estimated using the test indices. To eliminate errors, five groups of data were selected, and the average values were calculated. The field experiment results are presented in Table 6.



Figure 9 Field experiment

The results indicated that the maximum weeding rate was 86.1%, minimum weeding rate was 83.9%, and average weeding rate was 85.2%; the maximum rice seedling damage rate was 5.7%, minimum rice seedling damage rate was 3.9%, and average rice seedling damage rate was 4.8%; the maximum working fuel consumption was 15.3 L/hm², minimum working fuel consumption was 13.4 L/hm², and average working fuel consumption was 14.3 L/hm². The paddy field experiments verified that the weeding machine designed in this study met the design requirements for paddy weeding devices.

Table 6 Field experiment results

Test No.	Weeding Rate/%	Rice seedling damage rate/%	Working fuel Consumption/L hm ⁻²
1	84.7	3.9	14.6
2	85.6	5.3	13.5
3	86.1	4.2	15.3
4	83.9	5.7	13.4
5	85.7	5.0	14.7
Average	85.2	4.8	14.3

6 Conclusions

A weeding machine for paddy fields was designed, and the structural parameters of the weeding wheel, such as the width, radius, the number and length of rake teeth, were determined by analyzing the working principles and moving process of the weeding wheel. The influencing factors on the weeding torque in a descending order are rotation speed of the weeding wheel, hoeing depth, and forward speed of the device. The influencing factors on the soil disturbance speed in a descending order are rotation speed of the weeding wheel, hoeing depth, and forward speed of the device. A multi-index comprehensive weighted scoring method was used to comprehensively evaluate the simulation experiment results, and it was concluded that a better performance of the weeding wheel could be obtained when the hoeing depth was 50 mm, rotation speed of the weeding wheel was 240 r/min, and forward speed of the device was 0.6 m/s. The field experiment results revealed that the weeding machine could meet the design requirements for paddy weeding devices.

Acknowledgements

The project was supported by the National Natural Science Foundation of China (Grant No. 51475002) and the Major Science and Technology projects of Anhui Province (Grant No. 17030701046) and the Natural Science Foundation of Anhui Province (Grant No. 2008085QE270; 1808085QE171).

[References]

- [1] Bond W, Grundy A C. Non-chemical weed management in organic farming system. *Weed Research*, 2001; 41(5): 383–405.
- [2] Chen Z W, Zhang C L, Li N, Sun Z. Study review and analysis of high performance intra-row weeding robot. *Transactions of the CSAE*, 2015; 31(5): 1–8. (in Chinese)
- [3] Wang J F, Wang J W, Yan D W, Zhou W. Design and experiment of 3SCJ-2 type row weeding machine for paddy field. *Transactions of the CSAM*, 2017; 48(6): 71–78, 202.
- [4] Usui T, Ito K, Osato T. Weeding effect of fixed tine type weeding machine in rice cultivation. *Tohoku Weed Research Society*, 2009; 9: 38–41.
- [5] Minoru Sangyo Co., Ltd. Weeding machine. Japan; 4038538, 2007-11-16.
- [6] Wado Sangyo Co., Ltd. Paddy weeding machine. Japan; 4057492, 2007-12-21.

- [7] Ishii H, Sato M. Measures to improve the performance of weeding machines for paddy field tillage and to improve the weeding effect. *Bulletin of the Kanto Branch of the Crop Science Society of Japan*, 2006; (21): 22–23.
- [8] Agriculture and Food Technology Research Institute, Kubota Corporation, Iseki Agricultural Machinery Co., Ltd. Paddy weeding machine. Japan; 3965430, 2007-06-08.
- [9] Qi L, Ma X, Tan Z T, Tan Y. Development and experiment of marching-type inter-cultivation weeding machine for paddy. *Transactions of the CSAE*, 2012; 28(14): 31–35. (in Chinese)
- [10] Wang J W, Li C, Li X. Design and experiment of 3scj-1 type weeding machine for paddy field applied to film mulching and transplanting. *Transaction of the CSAM*, 2018; 49(4): 102–109. (in Chinese)
- [11] Qi L, Zhao L L, Ma X, Cui H, Zheng W, Lu Y. Design and test of 3gy-1920 wide-swath type weeding-cultivating machine for paddy. *Transactions of the CSAE*, 2017; 33(8): 47–55. (in Chinese)
- [12] Qi L, Liang Z W, Jiang Y, Ma X, Wu T, Lu Y L, et al. Design and field test of lightweight paddy weeding machine. *Journal of Jilin University (Engineering and Technology Edition)*, 2016; 46(3): 1004–1012. (in Chinese)
- [13] Ma Y J, Wang A, Zhao J G. Simulation analysis and experiment of drag reduction effect of convex blade subsoiler based on discrete element method. *Transactions of the CSAE*, 2019; 35(3): 16–23. (in Chinese)
- [14] Cundall P A, Strack O D L. A DISCRETE NUMERICAL MODE FOR GRANULAR ASSEMBLIES. *Géotechnique*, 1979; 29(1): 47–65.
- [15] Shmulevich I, Horn R. State of the art modeling of soil-tillage interaction using discrete element method. *Soil Tillage Research*, 2010; 111(1): 41–53.
- [16] Ucgul M, Fielde J M, Saunders C. 3D DEM tillage simulation: validation of a hysteretic spring (Plastic) contact model for a sweep tool operating in a cohesionless soil. *Soil Tillage Research*, 2014; 144: 220–227.
- [17] Yang L, Peng J, Yang H Y. Three-dimensional growth modeling of rice root based on differential 1-system. *Transaction of the CSAM*, 2019; 50(10): 208–214. (in Chinese)
- [18] Yang S M. Design and experiment of the key components for rice cultivation. PhD dissertation. Harbin: Northeast Agricultural University, 2013. (in Chinese)
- [19] Xu S X, Xu X B, He Y K. Morphology and anatomy of rice. Beijing: Agricultural Press, 1984. (in Chinese)
- [20] Zhou Y Z, Wang W X, Cheng L M, Zeng Y J, Tan X M, Hu S X, et al. Research progress of weed occurrence and control in direct seeding rice field. *Crops*, 2019; 35(4): 1–9. (in Chinese)
- [21] Zhang J L, Wu S, Shi X G, Li B T, Tang L M. Influence of Barnyardgrass (*Echinochloa crusgalli*) on the growth of double-cropping paddy rice and its economic threshold. *Acta Prataculturae Sinica*, 2015; 24(8): 44–52.
- [22] Zhu W D, Zhou P G, He Y H, Yang J, Lin R H, Qi W Q, et al. Influence of *Leptochloa Chinensis* (L.) Nees. on growth and yield properties of rice and its economic threshold of control. *Journal of Southern Agriculture*, 2018; 49(5): 863–869. (in Chinese)
- [23] Tao G X, Wang J W, Zhou W Q, Niu C L, Zhao J K. Herbicidal mechanism and key components design for paddy weeding device. *Transactions of the CSAM*, 2015; 46(11): 57–63. (in Chinese)
- [24] Wu C Y, Zhang M, Jin C Q, Tu A. Design and experiment of 2BYS-6 type paddy weeding-cultivating machine. *Transaction of the CSAM*, 2009; 40(7): 51–54. (in Chinese)
- [25] Wang J F, Gao G B, Yan D W, Weng W. Design and experiment of electric control double row deep fertilizing weeding machine in paddy field. *Transaction of the CSAM*, 2018; 49(07): 46–57. (in Chinese)
- [26] Li N, Chen Z W, Zhu C B, Zhang C. System design and experiment of electric driven weeding robot. *Transaction of the CSAM*, 2016; 47(5): 15–20, 69. (in Chinese)
- [27] Zhang S, Du Y F, Zhu Z X, Mao E. Integrated control method of traction & slip ratio for rear-driving high-power tractors. *Transactions of the CSAE*, 2016; 32(12): 47–53. (in Chinese)
- [28] Siniakov P. The theory and calculation of soil farming machinery. In: Li Q G, Gao E G, Zhang X D, et al. (Ed.), editors. Beijing: China Agricultural Machinery Press, 1981; 256p. (in Chinese)
- [29] Zhang R, Han D L, Ji Q L, He Y, Li J Q. Calibration methods of sandy soil parameters in simulation of discrete element method. *Transaction of the CSAM*, 2017; 48(3): 49–56. (in Chinese)
- [30] Li Y X, Li F X, Xu X M, Shen C, Meng K, Chen J, et al. Parameter calibration of wheat flour for discrete element method simulation based on particle scaling. *Transactions of the CSAE*, 2019; 35(16): 320–327. (in Chinese)
- [31] Ding Q S, Ren J, Adam B E, Zhao J. DEM analysis of subsoiling process in wet clayey paddy soil. *Transaction of the CSAM*, 2017; 48(3): 38–48. (in Chinese)
- [32] Wu T, Huang W F, Chen X S, Ma X, Han Z, Pan T. Calibration of discrete element model parameters for cohesive soil considering the cohesion between particles. *Journal of South China Agricultural University*, 2017; 38(3): 93–98. (in Chinese)
- [33] Waters J F, Lee S, Guduru P R. Mechanics of axisymmetric wavy surface adhesion: JKR-DMT transition solution. *International Journal of Solids and Structures*, 2008; 46(5): 1033–1042.
- [34] Wu L Y, Qi S, Song Y Q, Xin M J, Liu C H, Kong A J, et al. A DEM analysis on drag reduction characteristics of paddy field machinery surface with bionic micro architectures. *Journal of Shenyang Agricultural University*, 2017; 48(1): 55–62. (in Chinese)
- [35] Qi L, Liang Z W, Ma X, Tan Y. Validation and analysis of fluid-structure interaction between rotary harrow weeding roll and paddy soil. *Transactions of the CSAE*, 2015; 31(5): 29–37. (in Chinese)
- [36] Yu W J, Jia C, Di S T, Li K, Yuan H. Groundwater quality assessment based on comprehensive weight and improved matter-element extension evaluation model. *Journal of Jilin University (Earth Science Edition)*, 2019; 49(2): 539–547. (in Chinese)